Hindawi
Advances in Condensed Matter Physics
Volume 2018, Article ID 2849175, 9 pages
https://doi.org/10.1155/2018/2849175

Research Article

Single File Flow of Biomimetic Beads for Continuous SERS Recording in a Microfluidic Device

Diego Calzavara,[1,2] Davide Ferraro,[1] Lucio Litti,[2] Greshia Cappozzo,[1,2] Giampaolo Mistura,[1] Moreno Meneghetti,[2] and Matteo Pierno[1]

[1]*Dipartimento di Fisica e Astronomia "Galileo Galilei", Università di Padova, Via Marzolo 8, 35131 Padova, Italy*
[2]*Dipartimento di Scienze Chimiche, Università di Padova, Via Marzolo 1, 35131 Padova, Italy*

Correspondence should be addressed to Moreno Meneghetti; moreno.meneghetti@unipd.it
and Matteo Pierno; matteo.pierno@unipd.it

Received 31 January 2018; Revised 3 May 2018; Accepted 6 May 2018; Published 20 June 2018

Academic Editor: Mohindar S. Seehra

A major challenge in cancer treatment is the quantification of biomarkers associated with a specific cancer type. Important biomarkers are the circulating tumor cells (CTCs) detached from the main cancer and circulating in the blood. CTCs are very rare and their identification is still an issue. Although CTCs quantification can be estimated by using fluorescent markers, all the fluorescence techniques are strongly limited by the number of emissions (therefore markers) that can be discriminated with one exciting line, by their bleaching characteristics, and by the intrinsic autofluorescence of biological samples. An emerging technique that can overcome these limitations is Surface Enhanced Raman Scattering (SERS). Signals of vibrational origin with intensity similar to those of fluorescence, but narrower bandwidths, can be easily discriminated even by exciting with a single laser line. We recently showed the benefit of this method with cells fixed on a surface. However, this approach is too demanding to be applied in clinical routine. To effectively increase the throughput of the SERS analysis, microfluidics represents a promising tool. We report two different hydrodynamic strategies, based on device geometry and liquids viscosity, to successfully combine a microfluidic design with SERS.

1. Introduction

One of the most common techniques to characterize cells is cytofluorometry, which, in a continuous flow, allows detecting cells labeled with specific fluorescent probes. Up to thousands of cells per second can be processed. However, despite its rapidity, this technique is still limited to few detection channels because of the characteristic large bandwidths of fluorescence emissions and the use of different exciting lines for different fluorescent probes. In this scenario, Surface Enhanced Raman Scattering (SERS) [1] is a promising alternative because it shows intense signals, similar to those of fluorescence, but also very sharp bands, being of vibrational origin. This characteristic allows an easy multiplexing approach with many detected signals excited with only one laser line [1]. Furthermore, bleaching, which is a problem for fluorescence, is not present for SERS, and autofluorescence of biological samples does not disturb SERS signals. The enhancement of Raman scattering derives from the amplification of the local electromagnetic fields on the surface of plasmonic nanostructures. Optimized gold nanostructures, functionalized for cell targeting, were found to be good plasmonic nanostructures, useful to detect different populations of cancer cells [2, 3]. However, cells were fixed on a surface and analyzed one by one under a micro-Raman microscope, limiting the time analysis and, accordingly, the throughput of the system.

Microfluidics, which consists in the manipulation of liquids inside microchannels [4], due also to the simplicity of the typical microfabrication strategies [5–7], represents a promising platform to overcome this limitation, especially related to chemical [8, 9] and biomedical applications [10, 11]. As a matter of fact, during the past years, microfluidics showed capabilities in performing several biomedical applications regarding nucleic acid [12–15], immunoassays [16–19], and cell manipulations [20, 21].

Examples of microfluidic devices coupled with Raman spectroscopy have been successfully used for sample preconcentration or storing cells during the spectroscopic analysis [22–24].

For example, dielectrophoresis (DIE) is largely used for manipulating particles in microfluidic devices [25, 26] and, more recently, this approach has been recently combined with SERS analysis [27], for detection of specific biomarkers [28] and cells [29]. However, although DIE offers the advantage of precisely positioning cells or particles in the channel, it requires devices with integrated electrodes showing specific geometry, increasing the complexity and the cost of the microfabrication processes, and preventing the production of disposable device [30]. A passive approach that requires simpler fabrication protocols is represented by the use of a flow-focusing geometry to align cells (or particles) in a single line and force them to pass under the Raman laser spots, similarly to what is shown with UV-visible spectroscopy in flow [31]. However, only one work has been presented so far to push forward the flow-focusing geometry, with SERS analysis [32]. In fact, while this device allowed acquiring continuously the signal from flowing cells, it presents two main drawbacks: first, the usability of this procedure is severely limited by the acquisition time of SERS spectrometers (given by the CCD exposure and shutter). In addition, even with fast spectrometers (100-150 ms of acquisition time), it is necessary to design the microfluidic devices to reduce the velocity of the carrying flow. Since this achievement is commonly obtained by reenlarging the carrying flow after single file confinement [33], it has been demonstrated that beads flowing in a microfluidic device can be laterally displaced according to their size and stiffness [34, 35]. This may introduce some uncontrolled deviation from the laser spot, an issue when dealing with clinical analysis.

Given that the fluidic manipulation of cells (or beads) at slow speed in a microfluidic device is highly demanding since it requires working at very low pressure (typically hundreds of Pa), causing nonstable flows, a different approach can exploit the viscosity μ of the carrier fluid solution.

Within this approach, it is possible to affect the hydraulic resistance R_h of the microfluidic device and so the final flow rate. As a matter of fact, in a microchannel, once fixed the pressure drop ΔP at the channel ends, and the flow rate φ can be calculated as [36]

$$\varphi = \frac{\Delta P}{R_h} \tag{1}$$

R_h for a microfluidic channel of length L and radius r can be approximated as [37]

$$R_h = \frac{8\mu L}{\pi r^4} \tag{2}$$

Therefore, with fixed geometry, an increase of μ leads to a proportional increase of R_h and thus a reduction of the global flow rate in the device (see (1)).

We believe that both strategies for reducing the cells speed are interesting and both show advantages and disadvantages: (i) changing the geometry is very simple in the fabrication step; however it leads to a nonperfect straight trajectory of the cells; (ii) acting on the viscosity of the liquid could be not always possible; however, it permits working with a narrowed confined flow and thus a deterministic path of the cells. In this paper, we will compare the two strategies, demonstrating how even the latter one can be exploited to perform SERS in a microfluidic device. We used, for proof-of-concept experiments, biotinylated polystyrene beads (PS beads) as cell model [38, 39]. SERS nanostructures produced with gold nanoparticles, functionalized with an optimized SERS reporter ($NPCy(SH)_2$), were also functionalized with streptavidin. The biotin presented on the PS beads and the streptavidin on the gold nanostructures represent the antigen-antibody pair, used for the identification of cancer cells.

First, we introduce the methods for the fabrication of the microfluidic devices, the production of the SERS active nanostructures, and the experimental setup. Then, we report the numerical and experimental results for the fluidic characterization and we demonstrate the possibility of performing SERS analysis of beads flowing in the microfluidic device. Finally, we conclude comparing the two fluidic strategies and the results.

2. Materials and Methods

2.1. Microfluidic Device Fabrication and Liquid Handling. The microfluidic device was produced by conventional replica molding [5, 40] with polydimethylsiloxane (or PDMS, Sylgard 184, by Dow Corning) of a mold prepared by photolithography with SU-8 (by MicroChem). In detail, after having produced the mold, the nonpolymerized PDMS was poured on it and placed in an oven at 70°C for 1h. After that, the PDMS part was peeled off, punched for inlets, and bonded to a glass slide by Oxygen Plasma treatment. Finally, PTFE tubing having 0.3mm (0.6mm) inner (outer) diameter (by Sigma Aldrich) were fixed by epoxy glue as shown in Figure 1(a). The final design, described in Figure 1(b), shows a flow-focusing junction aimed at creating a focused flow in the center channel. The device presents two inlets' channel: one for the carrier liquid used to generate the confined flow and the other for the liquids containing the functionalized beads; both have the same cross section: 100μm ×20μm of lateral and thickness dimensions, respectively. Then, after the junction, the narrow channel opened in a larger chamber (w=700μm), aimed at reducing the flow rate and thus the speed of the beads. However, as introduced before, the confined stream flow in the chamber is larger than in the channel (see Figure 1(b)) and thus the beads position becomes less determined (see also Movie S1 in Supplementary Materials).

In order to optimize the focusing condition and characterize the speed of the beads, different glycerol/water mixes were used as carrier fluid, varying the viscosity between 1 and 120 cP; then, during the flow characterization experiments, the inner fluid was composed of non-coated polystyrene (PS) beads (size: 8.0-12.9μm, by Spherotech) dispersed in a Percoll/water solution (by GE Healthcare) at 42% w/w. The latter was used to match the density of the PS beads in order to reduce the sedimentation.

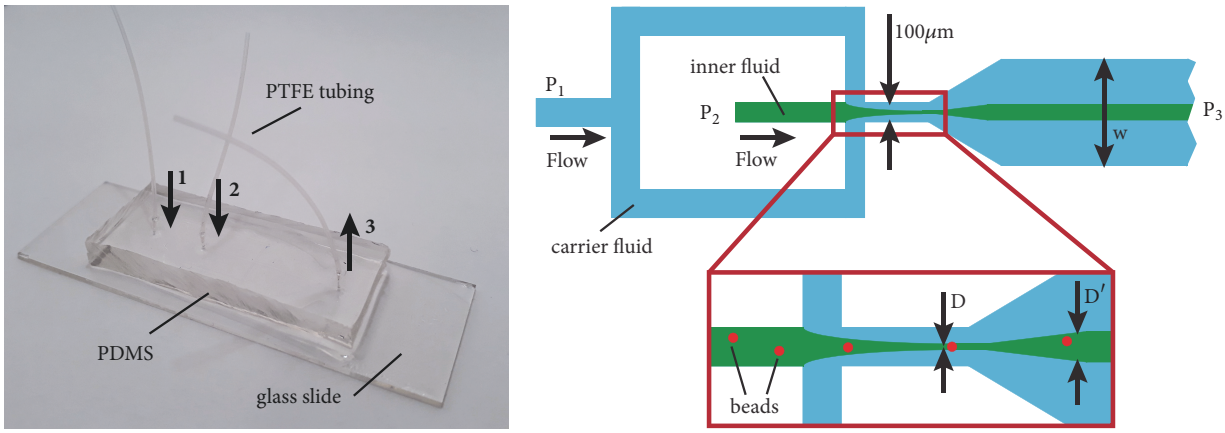

FIGURE 1: (a) Picture of the microfluidic device presenting inlets (1,2) and outlet (3). (b) Scheme of the microfluidic device: the carrier liquid (light blue) confines the inner fluid (green) that contains the PS beads (red spots). The scheme shows that the focusing is more efficient in the channel region (D) than in the chamber part (D′). P_1, P_2, and P_3 are the pressure corresponding to the inlets/outlet shown in (a).

The liquids in the microfluidic device were manipulated by an external pressure controller (MFCS by Fluigent) and the applied pressure was varied between 0.1kPa and 2.5kPa, in order to find the best condition for the flow confinement (see "D" in Figure 1(b)).

2.2. Polystyrene Beads for SERS Detection Preparation

(i) Streptavidin Functionalization with a Thiol Group. Streptavidin was thiolated using a procedure already reported [2]. Briefly, the protein is mixed with 2-iminothiolane (1:10 ratio) in a 0.1 M $NaHCO_3$ solution. The reaction proceeded for 2 hours at room temperature and at 4°C overnight. The mixture was purified by dialysis and dispersed in PBS.

(ii) AuNS Synthesis. Gold nanoparticles were synthetized by laser ablation, producing highly pure and stable colloids as previously reported [41]. In detail, a Nd:YAG (Quantel) laser at 1064 nm with 9 ns pulses and 10 Hz repetition rate was focalized on the surface of 99.99% pure gold plate at the bottom of a flask filled with 1 μM NaCl aqueous solution. 100 μL of 30 μM $NPCy(SH)_2$ [42] was added to functionalize and aggregate the particles (AuNS). A controlled aggregation allows producing hot spots in AuNS, where the SERS signal is strongly enhanced. The unreacted $NPCy(SH)_2$ was separated by centrifugation. The nanostructures were further functionalized with the thiolated streptavidin. The mixture was stirred for 3 hours at room temperature and left at 4°C overnight. The nanostructures were then purified by centrifugation. UV-vis-NIR (Cary 5000, Agilent) and μ-Raman (InVia, Renishaw) spectroscopies were used to characterize the nanostructures.

(iii) Incubation of AuNS with PS Beads. Biotinylated PS beads (size: 8.0-12.9μm, by Spherotech) were mixed with the functionalized AuNS and left for 4 hours at room temperature. Then, the mixture was centrifuged at 1000 RCF for 3 minutes. The supernatant containing the unreacted AuNS was discarded and the centrifuged PS@AuNS dispersed in the Percoll/water solution, as for the flow characterization part.

(iv) SERS Measurements of Flowing PS@AuNS. For the continuous SERS measurements, the 785 nm laser line at about 30 mW was focused on the middle of the sample channel with a 20× magnification objective. The acquisition was continuous at a repetition rate of 1 Hz. The dataset was baseline subtracted and each spectrum filtered for the intensity at 688 cm^{-1}. The data analysis was obtained with homemade Matlab™ codes.

3. Results and Discussion

3.1. Optimization of the Flow-Focusing Condition. At first, we investigated the best pressure conditions in order to obtain a narrow flow in the center of the channel. As a matter of fact, this is a fundamental aspect to obtain an aligned set of beads passing one by one in a specific detection region. Figure 2 describes the lateral size of the focused flow as a function of the ratio between the applied pressure P_2/P_1, keeping fixed P_3 at 0.5kPa. In order to perform this experiment, a fluorescein/Percoll solution was used in the inner channel and observed by a fluorescent microscope. It is possible to notice that the trend is almost linear in the investigated region and in particular, for values below 0.5, D is smaller than 20 μm, which corresponds to twice the beads size. Therefore, in order to ensure stable pressure control and a narrow flow, we fixed their values at P_1=2.5kPa, P_2=1.0kPa, and P_3=0.5kPa (P_2/P_1=0.4). Finally, those values were kept constant in all the following experiments, in order to evaluate only the influence of the viscosity on the beads' speed.

3.2. Size of the Microfluidic Chamber. The influence on the local speed of the lateral size (w) of the microfluidic chamber was first evaluated, keeping the applied pressure fixed (see Figure 3(a)). We performed different numerical simulation (with Comsol Multiphysics™), varying w and measuring the

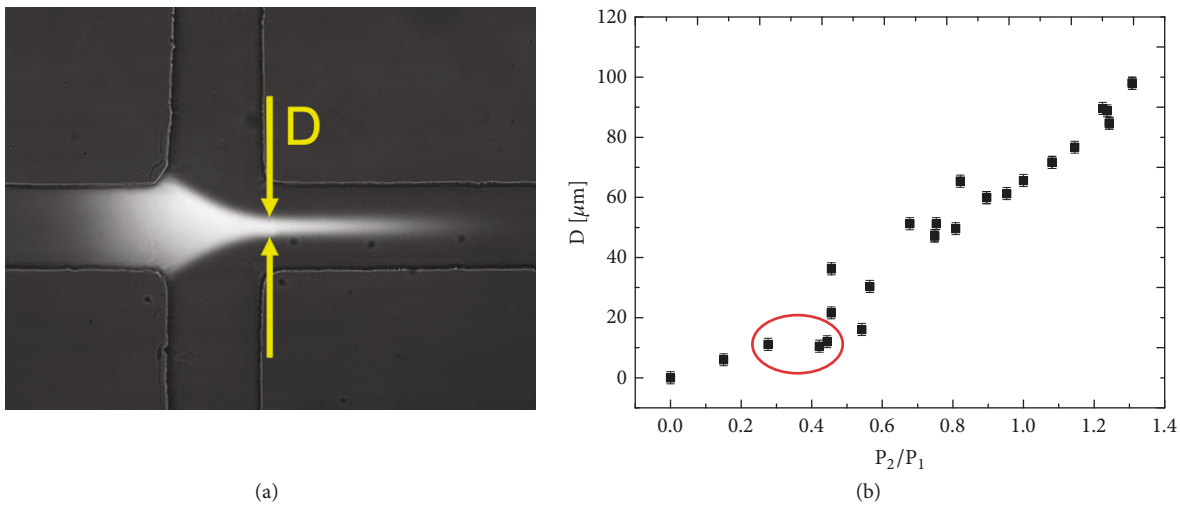

FIGURE 2: (a) Fluorescent image of the flow-focusing, with the fluorescein mix used as inner solution. (b) Dimension of D as function of the pressure ratio P_2/P_1; the red circle underlines the selected region for the following experiment.

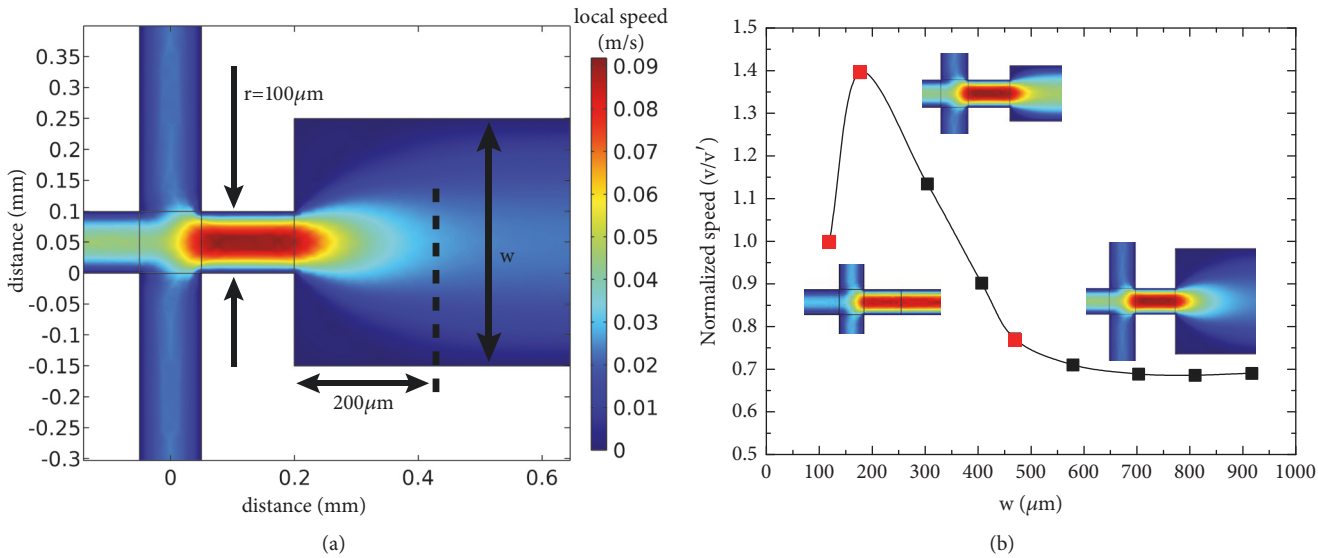

FIGURE 3: (a) 2D surface plots results of the local speed in the used microfluidic channels, for a particular value of w. (b) Normalized local speed of the liquid considered 200μm from the end of the channel and in the center of the chamber, plotted as function of its lateral dimension w. The reported simulation results correspond to the red data close to them. The local speed (v) was normalized by the speed obtained for the condition of a straight channel (v′), without the chamber (w=100μm).

droplet speed at 200 μm from the main channel after the focusing (vertical dashed line in Figure 3(a)). Figure 3(b) describes the droplet speed of the beads flowing in the center of the device, as a function of the lateral size of the fluidic chamber. All the speeds are normalized by the speed evaluated for a straight channel (w=r=100μm). It is possible to notice that, by increasing w, the speed initially increases up to 1.4 and then decreases reaching a plateau at about 0.7, and it is reduced to 1/3 of the initial value. This behavior can be explained by considering that, working at a fixed pressure, the increase of w leads to two contributions: (i) a reduction of the hydraulic resistance of the device that brings an increase of the flow rate and thus of the speed; (ii) an increase of the section of the device that causes a local speed reduction. Therefore, the observed effect is a balance between these two contributions. Observing the graph, at the beginning, the former contribution is more important, while for w>350μm, the latter one is dominant. Finally, over a certain value, the increase of the chamber size does not have any effect. In the microfabrication process we have chosen w=700 μm for our device in order to be in the plateau region.

3.3. Comparison between the Use of the Chamber and the Viscous Liquid. As introduced above, another strategy to reduce the beads speed in the microfluidic device is to increase the viscosity μ of the carrier fluid. Figure 4 shows the experimental results obtained by varying the viscosity of the

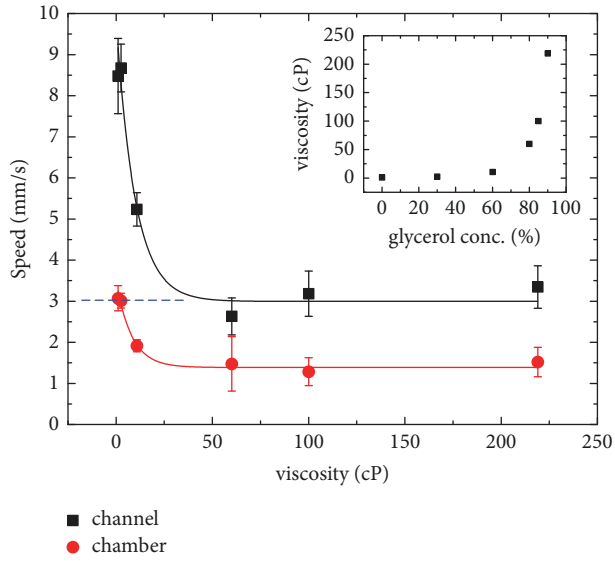

FIGURE 4: Speed of a beads evaluated in the center of the microfluidic device, in the channel (black data) and in the chamber (red data), plotted as function of the viscosity of the carrier liquids. The reported speeds are the averaged results of data for at least 5 beads and the error bars are the related standard deviation. The liquid viscosity was varied by different mix of water and glycerol (see inset).

carrier fluid in the main channel and in the large chamber. At first, for low viscosity ($\mu \geq 1$), the ratio between the two regimes is about 1/3 (chamber/channel≃3/9), similar to the one obtained by the Comsol simulation which considered pure water solutions instead of the beads/Percoll mixture. Then, taking into account the effect of the viscosity only in the channel, we can observe that, for $\mu \geq 25$, the speed of the beads decreases filling this gap, reaching the same value obtained in the chamber for low viscosity (see dashed line in Figure 4). This result shows that in the case of confined flow, only acting on the viscosity of the carrier fluid, it is possible to reduce the speed of the flowing beads, as much as changing the channel geometry. Additionally, as previously described, the presented approach allows a better confinement of the flowing beads than using a larger chamber.

After that, going deeper in the analysis, the beads can be additionally slowed down considering the effect of μ in the chamber part of the device. This suggests that combining the two contributions given by the geometry and the viscosity, it is possible to reduce the local speed by almost 10 times.

Finally, both trends reach a plateau at about 40 cP, probably due to the fact that for higher viscosity the flow of the carrier fluid does not change anymore at the fixed pressure (P_1=2.5kPa).

3.4. SERS Nanostructures and Model for SERS Labeled Cells. The above reported data were obtained with PS beads not labeled with AuNS. For the detection of SERS signals within the microchannel, PS beads were coupled with the streptavidin functionalized SERS-AuNS. Coupling PS beads with AuNS mimicked the interaction between cells and SERS label [38, 43].

At first, gold nanoparticles (AuNP) were produced by laser ablation synthesis in solution (LASiS), as previously reported for a wide range of materials [44–46]. Briefly, Nd:YAG nanosecond laser pulses were focused on a pure gold plate in a micromolar NaCl solution. Dithiolated silicon naphthalocyanine ($NPCy(SH)_2$) was used as SERS reporter to functionalize AuNP, due to its resonance with the exciting laser line at 785 nm. The function of the double thiol is to bridge the AuNP in order to achieve the maximum enhancement of the local field. Consequently, the SERS signals are strongly enhanced.

Finally, the AuNS were functionalized with the thiolated streptavidin using a previously reported protocol for antibodies [2, 47] as sketched in Figure 5(a). Figure 5(b) reports the extinction spectrum of the gold nanostructures (AuNS), which shows the good resonance with the 785 nm exciting laser line used for the μ-Raman measurements. Finally, Figure 5(c) shows the strong SERS spectrum of AuNS with the characteristic signature of $NPCy(SH)_2$, the band at 688 cm^{-1}, which will be used as the label of AuNS.

PS beads present already a coating of biotin that allows exploiting the interaction with streptavidin present on the functionalized AuNS. This allows simulating a typical strong binding between antigens and antibodies. AuNS and PS beads were mixed together at room temperature for 4 hours and the unbounded AuNS were discarded by centrifugation. The AuNS-PS beads conjugates were characterized by μ-Raman and TEM imaging. Every PS beads showed the SERS signature of Figure 5(c). TEM images (see Figure 6(a)) clearly showed AuNP aggregates on the surface of the PS beads. Finally, AuNS-PS beads were dispersed in Percoll solution and injected into the microfluidic device for the SERS detection (see Figure 6(b)).

3.5. Continuous SERS Detection in Microfluidic Device with Glycerol Solution as Carrier Fluid. The experiments to record

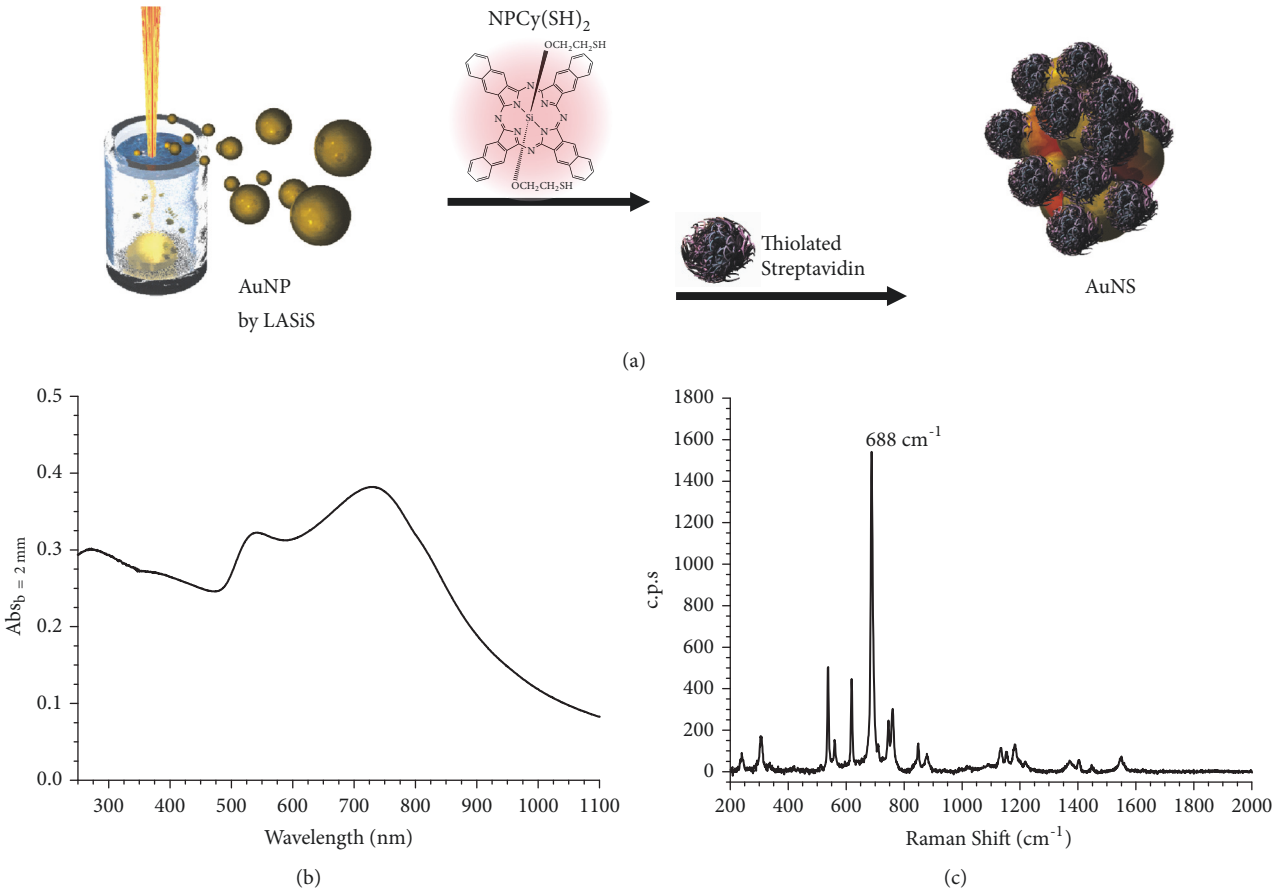

FIGURE 5: (a) Cartoon representing the synthesis of AuNS, from the laser ablation to the functionalization with the SERS reporter, NPCy(SH_2), and streptavidin. ((b) and (c)) UV-vis-NIR and SERS spectra of the functionalized AuNS, respectively.

SERS signals were performed using the AuNS-PS beads. The beads were flown at the previously characterized pressure (P_1=2.5kPa, P_2=1kPa, and P_3=0.5kPa) and focused in the center of the channel by the glycerol solution (80% w/w) as carrier liquid. As shown in Figure 4, in these conditions the beads speed was about 3mm s^{-1}, which was enough to be detected by the μ-Raman setup. Figure 6(c) describes the sequence of two images of the microfluidic device in which a PS bead was approaching the sampling area. The 785 nm laser of the μ-Raman was focused as a line on the center of the focused flow region, just after the focusing junction. Using a 20× magnification, the laser spot had a dimension of 100 μm ×5 μm. Raman spectra were acquired continuously, while the beads were flowing into the channel, at a frequency of 1 spectrum per second. The Raman band of PDMS at 710 cm^{-1}(green star in Figure 6(d)) was used to calibrate the focal position. The signal arising from the AuNS is clearly distinguishable at 688 cm^{-1}, marked as red star in Figure 6(d). From TEM images, as reported in Figure 6(a), one can estimate about 1.5% of AuNS surface coverage of a PS bead, which corresponds to about 10^2 nanostructures per bead. An example of a continuous flow measurement is presented in Figure 6(e), where the intensity at 688 cm^{-1} was monitored in time and the peaks marked with red stars are due to the bright SERS signals of AuNS at this specific wavelength. For example, the third peak of Figure 6(e), detected at about 815s, corresponds to the spectrum reported in Figure 6(d).

SERS signals of the AuNS are bright signals, which can be obtained with engineered nanostructures. The results show that these signals can be seen for the flowing PS beads labeled with the nanostructures and that they can be easily detected also with a conventional μ-Raman instrument.

4. Conclusions

By using a proper microfluidic approach, we showed the capability of achieving continuous SERS analysis by using a flow-focusing device. We reported two strategies aimed at slowing down PS beads in order to synchronize their passage times with the typical ones used in μ-Raman technology. Working either on the device geometry or the liquid viscosity, or on both of them, we proved a fine tuning of the beads speed flowing in a single file at low pressure regime. Targeted PS beads, used for mimicking targeted cells, are clearly identified with a continuous flow SERS analysis, showing that a microfluidic flow-focusing can be designed for controlling a flow of objects similar to cells, with density matched to the suspending medium, and that SERS signals deriving

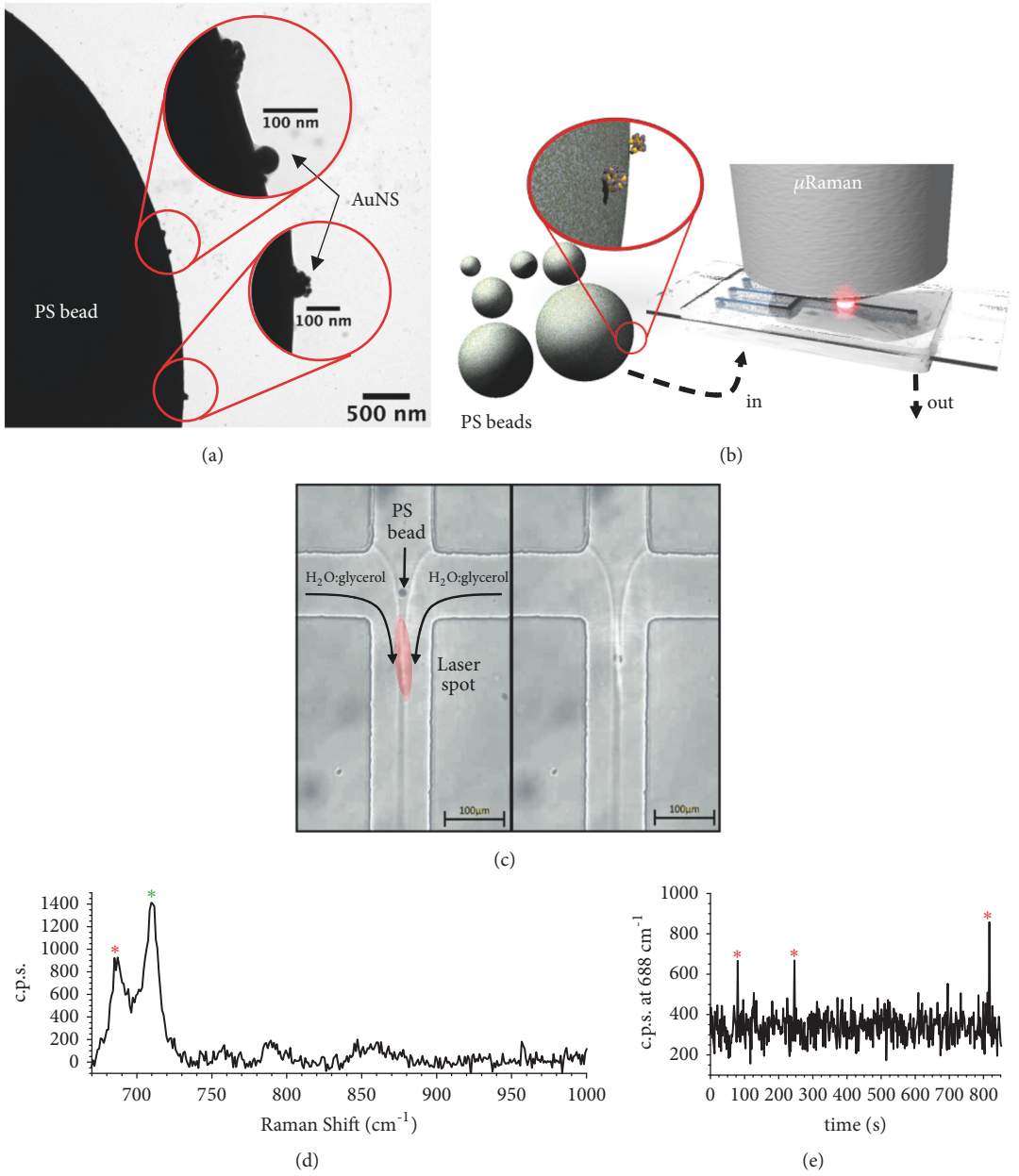

FIGURE 6: (a) TEM image of a AuNS targeted PS bead, little particles can be observed on the curvature, which are identified as AuNS in the inset magnifications. (b) Sketch of the objective of the μ-Raman over the microchannel. (c) Optical microscope images of the microfluidic device. A PS bead is caught just before entering on the sampling area (left). The elongated shape of the laser spot allows getting SERS signals from the AuNS-PS bead for a prolonged period (right). (d) Raman spectrum recorded at 815 s, where both the SERS-AuNS signal at 688 cm^{-1} and the PDMS peak at 710 cm^{-1} are observed. (e) Signals recorded at the fixed Raman shift of 688 cm^{-1} during the flowing of the nanoparticles in the microchannel.

from the targeting of these objects can be detected with a standard μ-Raman spectrometer. The two procedures present different advantages and disadvantages. In particular, the use of a viscous liquid as carrier fluid allows reducing the beads' speed similarly to what was obtained by introducing a downstream larger chamber with water or physiological buffers but ensuring better conditions for the confinement. The combination of the two approaches can be exploited to further reduce the speed down to 10 times with respect to the initial values. Overall, the most appropriate flow condition should be considered depending on specific applications. The possibility of doing multiplexing analysis with SERS signals excited with only one laser line was already proved and showed the potentiality of such a microfluidic device with respect to a cytofluorimetric device.

Data Availability

Data are available on request.

Disclosure

Greshia Cappozzo present address is as follows: Stevanato Group, Nuova Ompi S.r.l., Via Molinella 17, 35017 Piombino Dese (PD), Italy.

Conflicts of Interest

The authors declare that there are no conflicts of interest regarding the publication of this paper.

Acknowledgments

The authors kindly acknowledge Daniele Filippi, Dr. Paolo Sartori, Dr. Ladislav Derzsi, and Giorgio Delfitto for useful discussions and help in the experimental activities. Lucio Litti and Moreno Meneghetti would like to acknowledge the University of Padova funding P-DiSC no. 04BIRD2016-UNIPD and the Strategic Program of the University of Padova NAMECA.

Supplementary Materials

Movie S1: polystyrene beads flowing in the flow-focusing microfluidic device. Beads' path is well defined in the narrow channel by the flow-focusing, while it is less demarcated in the chamber. The movie is slowed down 15 times. *(Supplementary Materials)*

References

[1] S. Ding, E. You, Z. Tian, and M. Moskovits, "Electromagnetic theories of surface-enhanced Raman spectroscopy," *Chemical Society Reviews*, vol. 46, no. 13, pp. 4042–4076, 2017.

[2] M. Meneghetti, A. Scarsi, L. Litti et al., "Plasmonic nanostructures for SERRS multiplexed identification of tumor-associated antigens," *Small*, vol. 8, no. 24, pp. 3733–3738, 2012.

[3] F. Biscaglia, S. Rajendran, P. Conflitti et al., "Enhanced EGFR targeting activity of plasmonic nanostructures with engineered GE11 peptide," *Advanced Healthcare Materials*, vol. 6, no. 3, Article ID 1700596, 2017.

[4] G. M. Whitesides, "The origins and the future of microfluidics," *Nature*, vol. 442, no. 7101, pp. 368–373, 2006.

[5] Y. Xia and G. M. Whitesides, "Soft lithography," *Annual Review of Materials Research*, vol. 28, no. 1, pp. 153–184, 1998.

[6] E. Piccin, D. Ferraro, P. Sartori, E. Chiarello, M. Pierno, and G. Mistura, "Generation of water-in-oil and oil-in-water microdroplets in polyester-toner microfluidic devices," *Sensors and Actuators B: Chemical*, vol. 196, pp. 525–531, 2014.

[7] S. Silvestrini, D. Ferraro, T. Tóth et al., "Tailoring the wetting properties of thiolene microfluidic materials," *Lab on a Chip*, vol. 12, no. 20, pp. 4041–4043, 2012.

[8] D. Ferraro, Y. Lin, B. Teste et al., "Continuous chemical operations and modifications on magnetic γ-Fe_2O_3 nanoparticles confined in nanoliter droplets for the assembly of fluorescent and magnetic SiO_2@γ-Fe_2O_3," *Chemical Communications*, vol. 51, no. 95, pp. 16904–16907, 2015.

[9] N. Aboud, D. Ferraro, M. Taverna, S. Descroix, C. Smadja, and N. Thuy Tran, "Dyneon THV, a fluorinated thermoplastic as a novel material for microchip capillary electrophoresis," *Analyst*, vol. 141, no. 20, pp. 5776–5783, 2016.

[10] E. K. Sackmann, A. L. Fulton, and D. J. Beebe, "The present and future role of microfluidics in biomedical research," *Nature*, vol. 507, no. 7491, pp. 181–189, 2014.

[11] M. Serra, D. Ferraro, I. Pereiro, J.-L. Viovy, and S. Descroix, "The power of solid supports in multiphase and droplet-based microfluidics: Towards clinical applications," *Lab on a Chip* , vol. 17, no. 23, pp. 3979–3999, 2017.

[12] D. Ferraro, J. Champ, B. Teste et al., "Microfluidic platform combining droplets and magnetic tweezers: Application to HER2 expression in cancer diagnosis," *Scientific Reports*, vol. 6, Article ID 25540, 2016.

[13] C. D. Ahrberg, A. Manz, and B. G. Chung, "Polymerase chain reaction in microfluidic devices," *Lab on a Chip* , vol. 16, no. 20, pp. 3866–3884, 2016.

[14] A. K. White, M. VanInsberghe, O. I. Petriv et al., "High-throughput microfluidic single-cell RT-qPCR," *Proceedings of the National Acadamy of Sciences of the United States of America*, vol. 108, no. 34, pp. 13999–14004, 2011.

[15] I. Hernández-Neuta, I. Pereiro, A. Ahlford et al., "Microfluidic magnetic fluidized bed for DNA analysis in continuous flow mode," *Biosensors and Bioelectronics*, vol. 102, pp. 531–539, 2018.

[16] T. D. Mai, D. Ferraro, N. Aboud et al., "Single-step immunoassays and microfluidic droplet operation: Towards a versatile approach for detection of amyloid-β peptide-based biomarkers of Alzheimer's disease," *Sensors and Actuators B: Chemical*, vol. 255, pp. 2126–2135, 2018.

[17] G. Wang, C. Das, B. Ledden, Q. Sun, C. Nguyen, and S. Kumar, "Evaluation of disposable microfluidic chip design for automated and fast Immunoassays," *Biomicrofluidics*, vol. 11, no. 1, Article ID 014115, 2017.

[18] B. Teste, N. Jamond, D. Ferraro, J.-L. Viovy, and L. Malaquin, "Selective handling of droplets in a microfluidic device using magnetic rails," *Microfluidics and Nanofluidics*, vol. 19, no. 1, pp. 141–153, 2015.

[19] L. Mou and X. Jiang, "Materials for microfluidic immunoassays: a review," *Advanced Healthcare Materials*, vol. 6, no. 15, Article ID 1601403, 2017.

[20] L. Mazutis, J. Gilbert, W. L. Ung, D. A. Weitz, A. D. Griffiths, and J. A. Heyman, "Single-cell analysis and sorting using droplet-based microfluidics," *Nature Protocols*, vol. 8, no. 5, pp. 870–891, 2013.

[21] H. N. Joensson and H. Andersson Svahn, "Droplet microfluidics-A tool for single-cell analysis," *Angewandte Chemie International Edition*, vol. 51, no. 49, pp. 12176–12192, 2012.

[22] L. W. Yap, H. Chen, Y. Gao et al., "Bifunctional plasmonic-magnetic particles for an enhanced microfluidic SERS immunoassay," *Nanoscale*, vol. 9, no. 23, pp. 7822–7829, 2017.

[23] C. Wang, F. Madiyar, C. Yu, and J. Li, "Detection of extremely low concentration waterborne pathogen using a multiplexing self-referencing SERS microfluidic biosensor," *Journal of Biological Engineering*, vol. 11, article 9, 2017.

[24] Z. Zhai, F. Zhang, X. Chen et al., "Uptake of silver nanoparticles by DHA-treated cancer cells examined by surface-enhanced Raman spectroscopy in a microfluidic chip," *Lab on a Chip* , vol. 17, no. 7, pp. 1306–1313, 2017.

[25] K. Kalantar-Zadeh, K. Khoshmanesh, A. A. Kayani, S. Nahavandi, and A. Mitchell, "Dielectrophoretically tuneable optical waveguides using nanoparticles in microfluidics," *Applied Physics Letters*, vol. 96, no. 10, Article ID 101108, 2010.

[26] C. Zhang, K. Khoshmanesh, A. Mitchell, and K. Kalantar-Zadeh, "Dielectrophoresis for manipulation of micro/nano particles in microfluidic systems," *Analytical and Bioanalytical Chemistry*, vol. 396, no. 1, pp. 401–420, 2010.

[27] A. F. Chrimes, A. A. Kayani, K. Khoshmanesh et al., "Dielectrophoresis-Raman spectroscopy system for analysing suspended nanoparticles," *Lab on a Chip* , vol. 11, no. 5, pp. 921–928, 2011.

[28] A. F. Chrimes, K. Khoshmanesh, S.-Y. Tang et al., "In situ SERS probing of nano-silver coated individual yeast cells," *Biosensors and Bioelectronics*, vol. 49, pp. 536–541, 2013.

[29] A. F. Chrimes, K. Khoshmanesh, P. R. Stoddart et al., "Active control of silver nanoparticles spacing using dielectrophoresis for surface-enhanced Raman scattering," *Analytical Chemistry*, vol. 84, no. 9, pp. 4029–4035, 2012.

[30] J. Oakey, R. W. Applegate, E. Arellano, D. D. Carlo, S. W. Graves, and M. Toner, "Particle focusing in staged inertial microfluidic devices for flow cytometry," *Analytical Chemistry*, vol. 82, no. 9, pp. 3862–3867, 2010.

[31] J.-C. Baret, O. J. Miller, V. Taly et al., "Fluorescence-activated droplet sorting (FADS): Efficient microfluidic cell sorting based on enzymatic activity," *Lab on a Chip* , vol. 9, no. 13, pp. 1850–1858, 2009.

[32] A. Pallaoro, M. R. Hoonejani, G. B. Braun, C. D. Meinhart, and M. Moskovits, "Rapid identification by surface-enhanced raman spectroscopy of cancer cells at low concentrations flowing in a microfluidic channel," *ACS Nano*, vol. 9, no. 4, pp. 4328–4336, 2015.

[33] E. Locatelli, M. Pierno, F. Baldovin, E. Orlandini, Y. Tan, and S. Pagliara, "Single-File Escape of Colloidal Particles from Microfluidic Channels," *Physical Review Letters*, vol. 117, no. 3, Article ID 038001, 2016.

[34] A. Karimi, S. Yazdi, and A. M. Ardekani, "Hydrodynamic mechanisms of cell and particle trapping in microfluidics," *Biomicrofluidics*, vol. 7, no. 2, Article ID 021501, 2013.

[35] X. Xuan, J. Zhu, and C. Church, "Particle focusing in microfluidic devices," *Microfluidics and Nanofluidics*, vol. 9, no. 1, pp. 1–16, 2010.

[36] P. Tabeling, *Introduction to Microfluidics*, Oxford University Press, 2005, https://books.google.it/books/about/Introduction_to_Microfluidics.html?id=h4ZguvxYW0kC&redir_esc=y.

[37] D. Ferraro, M. Serra, I. Ferrante, J.-L. Viovy, and S. Descroix, "Microfluidic valve with zero dead volume and negligible backflow for droplets handling," *Sensors and Actuators B: Chemical*, vol. 258, pp. 1051–1059, 2018.

[38] W. Tan and S. Takeuchi, "A trap-and-release integrated microfluidic system for dynamic microarray applications," *Proceedings of the National Acadamy of Sciences of the United States of America*, vol. 104, no. 4, pp. 1146–1151, 2007.

[39] S. Kobel, A. Valero, J. Latt, P. Renaud, and M. Lutolf, "Optimization of microfluidic single cell trapping for long-term on-chip culture," *Lab on a Chip* , vol. 10, no. 7, pp. 857–863, 2010.

[40] E. Chiarello, A. Gupta, G. Mistura, M. Sbragaglia, and M. Pierno, "Droplet breakup driven by shear thinning solutions in a microfluidic T-junction," *Physical Review Fluids*, vol. 2, Article ID 123602, 2017.

[41] V. Amendola, L. Litti, and M. Meneghetti, "LDI-MS assisted by chemical-free gold nanoparticles: Enhanced sensitivity and reduced background in the low-mass region," *Analytical Chemistry*, vol. 85, no. 24, pp. 11747–11754, 2013.

[42] L. Litti, N. Rivato, G. Fracasso et al., "A SERRS/MRI multimodal contrast agent based on naked Au nanoparticles functionalized with a Gd(iii) loaded PEG polymer for tumor imaging and localized hyperthermia," *Nanoscale*, vol. 10, no. 3, pp. 1272–1278, 2018.

[43] M. R. Hoonejani, A. Pallaoro, G. B. Braun, M. Moskovits, and C. D. Meinhart, "Quantitative multiplexed simulated-cell identification by SERS in microfluidic devices," *Nanoscale*, vol. 7, no. 40, pp. 16834–16840, 2015.

[44] F. Lamberti, L. Litti, M. De Bastiani et al., "High-Quality, Ligands-Free, Mixed-Halide Perovskite Nanocrystals Inks for Optoelectronic Applications," *Advanced Energy Materials*, vol. 7, no. 8, 2017.

[45] F. Bertorelle, M. Pinto, R. Zappon et al., "Safe core-satellite magneto-plasmonic nanostructures for efficient targeting and photothermal treatment of tumor cells," *Nanoscale*, vol. 10, no. 3, pp. 976–984, 2018.

[46] V. Amendola, S. Scaramuzza, L. Litti et al., "Magneto-plasmonic Au-Fe alloy nanoparticles designed for multimodal SERS-MRI-CT imaging," *Small*, vol. 10, no. 12, pp. 2476–2486, 2014.

[47] G. Sciutto, L. Litti, C. Lofrumento et al., "Alternative SERRS probes for the immunochemical localization of ovalbumin in paintings: An advanced mapping detection approach," *Analyst*, vol. 138, no. 16, pp. 4532–4541, 2013.